Bimodal BCI Using Simultaneously NIRS and EEG

Yohei Tomita*, *Member, IEEE*, François-Benoît Vialatte, *Member, IEEE*, Gérard Dreyfus, *Fellow, IEEE*, Yasue Mitsukura, *Member, IEEE*, Hovagim Bakardjian, *Member, IEEE*, and Andrzej Cichocki, *Fellow, IEEE*

Abstract—Although noninvasive brain–computer interfaces (BCI) based on electroencephalographic (EEG) signals have been studied increasingly over the recent decades, their performance is still limited in two important aspects. First, the difficulty of performing a reliable detection of BCI commands increases when EEG epoch length decreases, which makes high information transfer rates difficult to achieve. Second, the BCI system often misclassifies the EEG signals as commands, although the subject is not performing any task. In order to circumvent these limitations, the hemodynamic fluctuations in the brain during stimulation with steady-state visual evoked potentials (SSVEP) were measured using near-infrared spectroscopy (NIRS) simultaneously with EEG. BCI commands were estimated based on responses to a flickering checkerboard (ON-period). Furthermore, an "idle" command was generated from the signal recorded by the NIRS system when the checkerboard was not flickering (OFF-period). The joint use of EEG and NIRS was shown to improve the SSVEP classification. For 13 subjects, the relative improvement in error rates obtained by using the NIRS signal, for nine classes including the "idle" mode, ranged from 85% to 53%, when the epoch length increase from 3 to 12 s. These results were obtained from only one EEG and one NIRS channel. The proposed bimodal NIRS–EEG approach, including detection of the idle mode, may make current BCI systems faster and more reliable.

Index Terms—Brain–computer interface (BCI), bimodal, simultaneous electroencephalographic (EEG) and near-infrared spectroscopy (NIRS), steady-state visual evoked potentials (SSVEP).

I. INTRODUCTION

DIRECT communication techniques enabling the exchange of information between the brain and computers such as brain–computer interfaces (BCIs) have been gaining momentum over the recent decades. One of the pioneering studies using monkeys was proposed in [1]. Although, in these early BCI experiments, the subject was not human, and a steel plug was permanently implanted over the precentral cortex, subsequent studies demonstrated the possibility of noninvasive analysis of the human brain due to the rapid development of neuroimaging modalities and signal processing techniques [2]–[4]. Currently, several noninvasive functional imaging modalities are available for research, such as electroencephalography (EEG), magnetoencephalography (MEG), functional magnetic resonance imaging (fMRI), and near-infrared spectroscopy (NIRS). They encompass the most active areas of BCI research [5].

Among these brain imaging modalities, EEG has most often been used for BCI due to the high temporal resolution of the measured brain signals, device portability, and low cost. Recently, coordinated scientific efforts have been made in order to develop EEG-based BCI systems, as can be illustrated by the emergence of open-access data and EEG-based BCI competitions (see for instance [6], [7]), which led to improvements of signal processing and classification algorithms. The short response times of the brain processes underlying EEG allow users to control an external device in near-real-time [8]–[10]. For instance, Hill and coauthors [11], in an evaluation of motor imagery based BCI, compared the performance of EEG, MEG, and electrocorticography recording modalities, and concluded that EEG allowed better general performance than the other modalities. Furthermore, Millán *et al.* proposed a mental task recognition technique using near-real-time spontaneous EEG signals: they were able to classify correctly three mental tasks with a success rate of 70% [12]. Other studies, based on P300 evoked potentials, obtained higher classification performance [13]. BCI systems based on steady-state visually evoked potentials (SSVEP) turned out to be very successful [14]–[17].

Nevertheless, improving EEG-based BCI performance is still a challenge. First of all, the reliability of command detection decreases as recording time decreases. The search for paradigms that can detect BCI commands with high temporal resolution is still active. In addition, most studies ignore BCI system behavior in an idle mode when the user does not require any action. In BCI systems, using visual stimuli, the subjects can activate a command by focusing his attention on one of several stimuli. However, in practice, it is not easy to focus attention for a long time, as subjects may become diverted, drowsy, or unwilling to look at the stimulation. Consequently, SSVEP BCIs often send signals when the user did not intend to convey anything (called false positives), which can be especially problematic during breaks or resting periods [18]. Such occurrences should be identified explicitly as an idle mode, otherwise the BCI system may erroneously issue a command.

To overcome these substantial limitations, we exploit simultaneously an additional source of information, namely the hemodynamic changes measured by NIRS. Recently, a wide variety

Fig. 1.   Principles of a bimodal BCI using EEG and NIRS simultaneously.

TABLE I
PREVIOUS STUDIES RELATED TO NIRS-BASED BCI

Authors	Modality	Task	NIRS Features
Coyle et al. [19]	NIRS	Motor imagery	Averaged concentration
Sitaram et al. [20]	NIRS	Motor imagery	Averaged concentration
Tai and Chau [21]	NIRS	Emotional induction	Mean, variance, and so on
Pfurtscheller et al. [18]	NIRS-EEG	Concentration (brain switch)	Moments (2nd to 4th order), mean, root-mean square, wavelet
Takeuchi et al. [22]	NIRS-EEG	Electrical stimulation	Peak response
Fazli et al. [23]	NIRS-EEG	Motor imagery	Averaged concentration

Motor imagery task is the most frequently used paradigm.

of NIRS devices has been made available. Expensive models feature numerous sensor probes and analysis tools, but quick medical examinations can be carried out with cheaper devices featuring a smaller number of probes. The advantages of NIRS are that it is impervious to the widely-spread environmental electrical noise and much less sensitive to EMG (muscle) artifacts than EEG. NIRS measures oxygenated hemoglobin (Hb) and deoxygenated Hb concentrations. In addition, the blood oxygenation level-dependent signal elicited by visual stimulation has been well described using fMRI [24], [25]. Blood Hb concentration changes have been clearly shown to be related to the presence and absence of the stimulation. Other studies using EEG, fMRI, and NIRS [19], [23], [26]–[28] lead to the conclusion that hemodynamic changes may be a promising indicator to overcome the limitations of the command detection. For instance, for a wheelchair control BCI, the detection of onset and offset responses improves the BCI usability—when the subject is not willing to execute a command, the wheelchair should not move.

Fig. 1 illustrates the joint use of EEG (for command detection) and NIRS (the detection of stimulation onset and offset) in a BCI system. In this study, we present such an approach and demonstrate its use in a BCI system based on SSVEP.

The organization of the paper is as follows. Section II gives details on the NIRS BCI and on NIRS signal processing. In Section III, the experimental protocol and the joint EEG—NIRS BCI design are presented. Sections IV, V, and VI contain results, discussions, and conclusions, respectively.

II. FEATURE EXTRACTION FOR HEMODYNAMIC RESPONSES

Before describing the joint EEG–NIRS BCI paradigm, we will first present a rationale for our approach based on some

previously published NIRS-based BCI techniques. New perspectives for NIRS–BCI could arise from these investigations although so far there have been only a few BCI studies using the NIRS recording modality as compared to EEG. The basic hemodynamic brain response, as well as the noise cancellation technique which is applied before the feature extraction step, are also explained in this section.

A. Existing NIRS–BCI Methods

Table I shows a summary of NIRS–BCI research publications. Many of these studies were based on motor imagery of finger and arm movements. They detected blood oxygenation responses (slow oscillations at 0.1–0.5 Hz) following motor imagery, and concluded that motor imagery was appropriate for NIRS–BCI applications [19]–[21]. On another hand, it was suggested that the reliability of NIRS—BCI could be improved by combining NIRS with other brain recording modalities. The concept of combining recording modalities is detailed in [18], [22], and [23]. For example in [23], the performance of a sensory motor rhythm based BCI was significantly improved by simultaneous measurement of EEG and NIRS. Another study with simultaneous recording of NIRS and EEG [22] measured the responses to electrical stimulation at the right median nerve, and concluded that evaluating NIRS and EEG simultaneously provided useful information.

In the present paper, we merge EEG and NIRS modalities in an SSVEP-based BCI. SSVEP is already a powerful paradigm for EEG-based BCI because responses to steady-state visual stimuli have a very good signal-to-noise ratio. The idea that NIRS could be used as a brain switch to turn ON or OFF the SSVEP detection in an SSVEP-based BCI is discussed in [18], but using a different approach—a cognitive NIRS response is
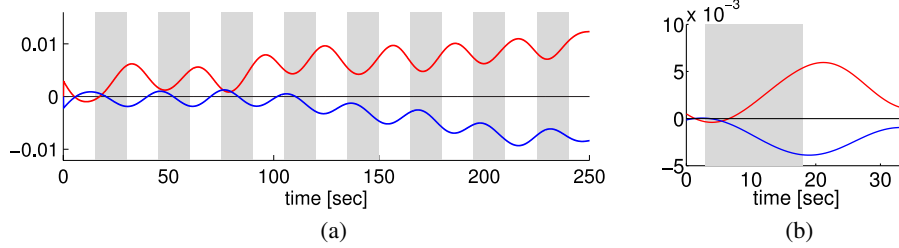
Fig. 2. Hemodynamic response changes (O_2Hb and HHb) corresponding to visual stimulations indicated by the gray colored periods (see Section III in details). (a) Block-averaged result for all 37 blocks after low-pass filtering (red: O_2Hb, blue: HHb) and (b) trial-averaged result for 37 (blocks) × 8 (trials of consecutive ON- and OFF-periods pairs). (a) Block averaging. (b) Trial averaging.
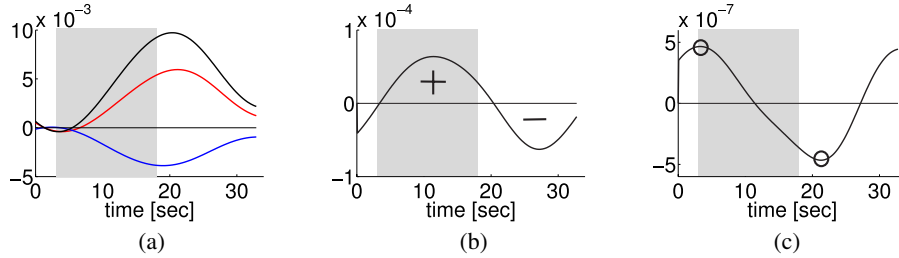
Fig. 3. Event related NIRS features. (a) Hemodynamic responses (red: O_2Hb, blue: HHb, black: O_2Hb-HHb). (b) and (c) show the 1st and 2nd derivatives of O_2Hb–HHb, respectively. Positive and negative of 1st derivative, and extrema of 2nd derivative are shown. (a) Hemodynamic response. (b) Derivative. (c) 2nd derivative.

detected in the prefrontal area, whereas we will focus in this paper on sensory responses in the occipital area. Indeed, NIRS studies of SSVEP brain responses show that even though the hemodynamic responses are slower, they do exhibit changes after stimulation onset and offset [29]. Therefore, the onset and the offset could be estimated by detecting the hemodynamic fluctuations in response to visual stimuli.

B. Hemodynamic Responses to SSVEP Stimulation

Changes in blood oxygenation accompany neural activity. Although they are slow and delayed with respect to neural activity, they convey information about the timing of neural activity. Hemodynamic signal changes due to SSVEP visual stimulation are affected by physical and physiological noise. In most offline studies, the noise is canceled out by averaging trials over time. Fig. 2(a), (b) show the changes of oxygenated Hb (O_2Hb) and of deoxygenated Hb (HHb) concentrations during steady-state visual stimulation. The signals were time-averaged for 37 trials in an experiment using pseudorandomly displayed stimuli (see Section III for details). Fig. 2 indicates that NIRS responses to the visual stimulation appear with a delay of 2–3 s after the beginning and the end of the stimulation.

Fig. 2 also shows that changes in O_2Hb and HHb are nearly symmetric. We make use of the first and second derivatives of the difference between the concentrations of oxygenated and deoxygenated hemoglobin O_2Hb–HHb [see Fig. 3(a), (b), and (c)]. The derivative is positive in most regions of the ON-period, and vice versa for the OFF-period. Moreover, an extremum of the second derivative can be detected at the beginning of each period. Therefore, the first and second derivatives may be useful features to detect the onset and offset of the visual stimulation.

C. Noise Reduction for NIRS Signal

NIRS signals are subject to noise, arising for instance from body movements, heart rate, and respiration effects [30]. For the purpose of BCI, noise components should be removed in real time from the hemodynamic signals. So far, NIRS signal noise removal algorithms have been implemented focusing on specific types of noise (cardiac, Mayer wave, and respiration). In many studies, noise-canceling algorithms have been investigated using methods such as the Kalman estimator for generalized linear models coefficient updating [31], least squares regression [32], wavelet-based filtering, independent component analysis [33], and adaptive filtering [33]–[35].

When investigating the properties of NIRS signal noise offline, phase-locked brain responses evoked by the same stimulation in multiple trials can be averaged in the time domain. Using this approach, one expects noise components to be canceled out because they are assumed to be additive of zero expectation value. Fig. 2 shows the signals averaged over $N = 37$ blocks:

$$\bar{x}(t) = \frac{1}{N} \sum_{i=1}^{N} x_i(t) \tag{1}$$

where $x_i(t)$ is the hemodynamic response at time t of the ith trial. The signal-to-noise ratio of a given NIRS event related potential is therefore enhanced when several trials are averaged. In order to evaluate the optimal frequency for the NIRS response to reversing checkerboards, we averaged all the trials in the Fourier domain. Letting $X_i(e^{j\omega})$ be the Fourier transform of a NIRS signal $x_i(t)$, the average Fourier power is

$$F(\omega) = |\bar{X}(e^{j\omega})| = \frac{1}{N} \left| \sum_{i=1}^{N} X_i(e^{j\omega}) \right|. \tag{2}$$
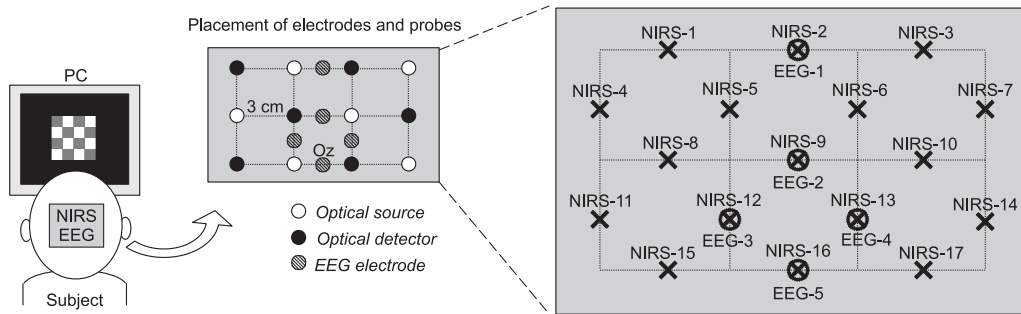
Fig. 4. EEG electrodes and NIRS probes are positioned in the occipital area. Each NIRS channel is located between an optical source and an optical detector. Four EEG electrodes are positioned at the same locations as the corresponding four NIRS channels (NIRS-2, NIRS-9, NIRS-12, NIRS-13, and NIRS-16).

We normalize this spectrum as follows:

$$R(\omega) = F(\omega)/G(\omega), \quad G(\omega) = \frac{1}{N}\sum_{i=1}^{N}|X_i(e^{j\omega})|. \quad (3)$$

The pulsation that maximizes $R(\omega)$ in (3), is the most relevant component, that we estimated at $\omega \approx 0.033$ Hz.

III. METHODS

Thirteen healthy subjects, who did not suffer from any brain disorder, with normal or corrected to normal vision, and who did not have any prior training participated in this experiment after signing written informed consent forms. The experimental design and the analysis methods for joint EEG–NIRS–BCI are detailed thereafter.

A. Recording and Stimulation

A special head cap was designed to record simultaneously the NIRS and EEG signals. This cap was flexible enough to fit the surface of the head. The head cap contained circular incisions for the EEG electrodes and similar incisions for the NIRS probes, placed over the occipital area as shown on Fig. 4. The distance between any two NIRS sensors was fixed at 3 cm. The EEG electrodes were placed between the NIRS sensors.

The setup of the NIRS instrument (OMM 3000, Shimadzu, Co. Ltd) consisted of six optical source probes (Near-IR semiconductor lasers) and six detector probes covering the occipital area. NIRS signals were recorded using pairs of neighboring source and detector probes. The midpoint between such a pair of probes was regarded as the probable location of the brain hemodynamic changes recorded by the corresponding NIRS channel. There were 17 NIRS channels (see the locations in Fig. 4), recorded with a sampling of 70 ms. All signals were passed through a digital Butterworth low-pass filter of order 3 and with a 0.04-Hz cutoff frequency. Hemodynamic changes were estimated for each NIRS channel using three different wavelengths (780 ± 5, 805 ± 5, and 830 ± 5 nm) and Hb concentration changes were estimated as O_2Hb, HHb, and total Hb change (O_2Hb+HHb) based on the modified Lambert–Beer law.

The experimental setup of the EEG system (V-amp, Brain Products GmbH) included six active electrodes. Before each recording, a small amount of gel was applied directly to the scalp to minimize the impedance (below 20 kΩ in our experiment) for all electrodes. 20 kΩ is a valid threshold when using active electrodes. The reference electrode was placed on the mandible bone near the left ear, and the ground electrode was placed at Cz according to the international 10/20 system. The most posterior electrode (EEG-5) was placed at Oz according to the international 10/20 system. All EEG measurement electrodes were positioned at the midpoint between the NIRS probes. This ensured that the locations of the EEG electrodes coincided with the locations of the NIRS channels. The sampling rate of the EEG recording was 500 Hz. All signals were passed through a digital Butterworth low-pass filter of order 3 and with a 40-Hz cutoff frequency, and a digital Butterworth high-pass filter of order 3 and with a 0.5-Hz cutoff frequency.

EEG and hemodynamic changes were recorded while the subjects focused on visual stimulations displayed on a screen. Subjects were seated 1.0 m from a 17-inch LCD computer display operated at a nominal refresh rate of 60 Hz. They were instructed to fix their gaze on a small cross appearing in the center of the screen. In this setup, the display had a 25-cm height, therefore the visual angle of the display was calculated to be 7.3° arc at most ($\theta \approx (25/2)/100$ rad). Continuous SSVEP stimulation was presented using reversing black-and-white checkerboards with 18×18 squares. A broad range of stimulation frequencies was presented (eight different reversing frequencies from 4.8 to 11.8 Hz): 4.8, 5.3, 5.8, 6.5, 7.3, 8.4, 9.8, and 11.8 Hz (see [17] for frequency optimization). All stimulation frequencies were displayed once each during a recording (defined as a block). A block had an overall duration of about 4 min. During each block, one trial for each of the eight possible reversal frequencies was recorded, with stimuli presented in a randomized order. During a given block, each stimulus was displayed for 15 s, followed by a 15 s period where the checkerboard pattern stopped reversing and remained still. We define as an "ON-period" the period of time when the checkerboard is reversing (whatever the stimulus frequency), and as an "OFF-period" the period of time when the checkerboard is not reversing. In a SSVEP BCI application, commands should be detected only when the subject is focusing on as stimulus, therefore during an ON-period (corresponding to a selective attention switch/gaze target change in a multistimulus system [17]). In this condition, SSVEP can be observed in response to the reversing pattern. During the OFF-period, the subject is not focusing on any command, and therefore the

system should clearly identify the event as an idle mode (no command). Subjects attended several recording sessions (each subject participated 2–4 times). Recording sessions were carried out on different days (two blocks maximum per day and per subject) to reduce fatigue effects. The number of the recording sessions varied due to the failure of some subjects to fulfill attention-related inclusion criteria: having enough sleep on the night before the recording, and not feeling tired before the experiment. A total of 37 blocks were recorded for all subjects (hence, 37 trials per stimulation frequency).

B. Feature Extraction

In this study, we intend to detect the difference between active and idle states using NIRS. We can observe (see Fig. 2) that O_2Hb increases after the beginning of stimulation and decreases after the end of stimulation, and vice versa for HHb. These variations in hemodynamic responses may be measured using temporal derivative estimations, which are efficient in extracting information during rapid transients. However, in the presence of high-frequency noise, temporal derivatives are prone to instabilities and inaccuracies. Therefore, we used a combination of low-pass and Savitzky–Golay (SG) filters to measure the variations of hemodynamic responses. The low-pass filter served to remove most noise components, and afterwards the derivative of the signal was estimated using the output of a SG filter. The basic idea of the SG filter is based on least-squares polynomial fitting. The polynomial of degree K is expressed as

$$p(t) = \sum_{k=0}^{K} a_k t^k \qquad (4)$$

where t^k represents the kth power of time t $(k = 0, \ldots, K)$, and the scalars a_k are the polynomial coefficients. The fitting of the coefficients a_k are performed by minimizing a cost function $\epsilon(t)$. Fitting curve is defined as

$$\hat{x}(t) = \underset{p(t)}{\operatorname{argmin}} \epsilon(t)$$

$$\left(\epsilon(t) = \int_{-M}^{M} \{p(t+\tau) - x(t+\tau)\}^2 d\tau \right) \qquad (5)$$

where $[-M, M]$ represents the time range centered on t for fitting. Then, temporal derivatives can be extracted such as

$$\frac{d}{dt}\hat{x}(t) = \sum_{k=1}^{K} k a_k t^{k-1} \qquad (6)$$

$$\frac{d^2}{dt^2}\hat{x}(t) = \sum_{k=1}^{K} k(k-1) a_k t^{k-2}. \qquad (7)$$

The active and the idle modes were estimated using the following workflow:

1) A low-pass filter was applied to extract slow NIRS oscillations with resulting signals $x_{O_2Hb}(t)$ and $x_{HHb}(t)$ [see Fig. 5(a)].
2) Define $y(t)$ considering O_2Hb and HHb changes, and its derivative as

$$y(t) = \hat{x}_{O_2Hb}(t) - \hat{x}_{HHb}(t) \qquad (8)$$
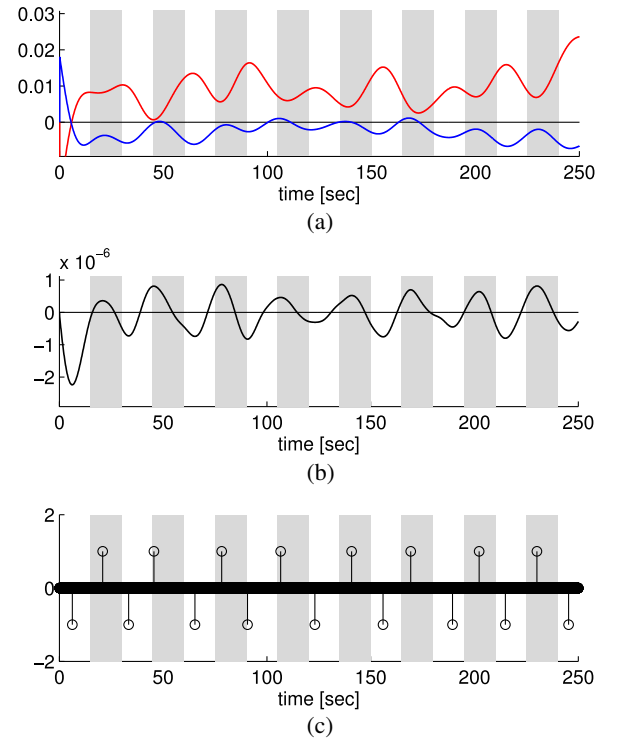
Fig. 5. Estimated onset and offset flags. (a) Low-pass-filtered signal from one trial data (red: x_{O_2Hb}, blue: x_{HHb}). (b) Difference of derivatives of x_{O_2Hb} and x_{HHb}. (c) Estimated onset and offset flags. Values of 1 and -1 represent the onset and offset flags, respectively. All calculated flags are extracted at their correct positions. (a) Noise canceled sample (x_{O_2Hb}, x_{HHb}). (b) $\frac{d^2}{dt^2}y$. (c) Detected flags.

$$\frac{d}{dt}y(t) = \frac{d}{dt}\hat{x}_{O_2Hb}(t) - \frac{d}{dt}\hat{x}_{HHb}(t). \qquad (9)$$

The derivatives of $y(t)$ was estimated using a SG filter with $M = 0.1$ s and $K = 2$. The difference of the second derivatives of $y(t)$ was also calculated [shown in Fig. 5(b)].

3) Onset flag and Offset flags were calculated for each time point t as shown in Fig. 5(c) when the following conditions using extrema were satisfied:

Onset flag:

$$S_{\text{onset}} = \Big\{ t \Big| \frac{d}{dt}y(t) > 0, \frac{d^3}{dt^3}y(t) = 0,$$

$$\frac{d^3}{dt^3}y(t^-) < 0, \frac{d^3}{dt^3}y(t^+) > 0 \Big\}. \qquad (10)$$

Offset flag:

$$S_{\text{offset}} = \Big\{ t \Big| \frac{d}{dt}y(t) < 0, \frac{d^3}{dt^3}y(t) = 0,$$

$$\frac{d^3}{dt^3}y(t^-) > 0, \frac{d^3}{dt^3}y(t^+) < 0 \Big\}. \qquad (11)$$

Here, the increase and decrease of the hemodynamic responses to SSVEP stimulation is expressed as $\frac{d}{dt}y(t)$. Moreover, the following three signal derivations ($\frac{d^3}{dt^3}y(t)$, $\frac{d^3}{dt^3}y(t^-)$, $\frac{d^3}{dt^3}y(t^+)$) were used to extract the beginning and the end of the stimulation based on the extremum of the second derivatives. These onset and offset flags were used to detect if the subject is
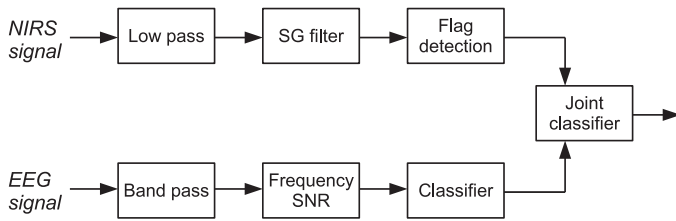
Fig. 6.   Block diagram of EEG and NIRS analysis consisting of an EEG analysis module, a NIRS analysis module, and a joint classification module.

in active or idle mode. There are two possible outcomes from this feature extraction procedure: either there is one flag only (either onset or offset flag), and in that case, a decision is taken (OFF or ON period is detected); or there are both flags and no flags in the analysis window, and in that case, no decision is taken (unknown condition). The NIRS signal analysis therefore led to a two-class classification, with a third output class (reject class).

C. Joint EEG–NIRS–BCI

In this study, SSVEP–BCI command classification was performed using simultaneous EEG and NIRS signals (see Fig. 6) in order to optimize the detection. For each trial, the NIRS signal was used to detect if the subject was in an active or idle mode. The EEG signal was used to estimate which command was to be activated. The system shall therefore detect either one of the eight possible commands, or an idle state.

The reversing checkerboard stimulation elicited SSVEP responses in the EEG signal, with peaks at the stimulus frequency as well as its harmonics. To detect SSVEPs, short EEG epochs (1-14 s) were extracted to compute the Fourier transform. In this study, the power spectrum of each trial was normalized by subtraction of the spectrum of the first OFF-period in each block. For command detection, only the fundamental frequency was used because the power of the other harmonics was not high enough to distinguish commands (the fundamental frequency provided the highest estimation accuracy). The SSVEP measurement was enhanced by computing the ratio of the Fourier power of the SSVEP peak to the Fourier power at neighboring frequencies, the so-called SSVEP signal-to-noise ratio (SSVEP SNR) [16].

From the EEG signal, a BCI command was estimated when the SSVEP response exceeded a threshold (± 0.1-Hz frequency centered at each stimulation frequency). First of all, the SSVEP SNR values were normalized by computing z-scores across all trials. Therefore, the normalized SNR peaks had an average value of 0 and a standard deviation of 1, whatever the frequency. The threshold parameter controlled the sensibility and specificity of BCI command detections. With a low threshold, BCI commands would be estimated at a higher rate, but with an increased risk of false detections during OFF-periods (a false positive). For a higher threshold, the risk of false detection was lower, but the BCI commands were estimated at a lower rate during the ON-period. We used two thresholds $1.0 \times$ std (std is the standard deviation calculated from the first OFF-period in

every block) as the lower threshold (TH1) and $2.3 \times$ std as the higher threshold (TH2).

The EEG features (command estimates) and NIRS features (onset and offset flags, described in Section III-B) were then fed into a joint classifier. One EEG and one NIRS channel with the best classification performance were selected (same channel for all subjects). As explained previously, the NIRS feature extraction led to a two-class classification (OFF- or ON-period) with a reject class (undetermined period). When an ON-period was detected, the command detection was based on the best command detected using EEG (regardless of the threshold). When an OFF-period is detected, an idle command is returned. When the reject output class is detected, the BCI command estimation is based on the best command detected using EEG, but taking into account a reject threshold (either TH1 or TH2) to detect the idle command. These thresholds were selected to compare sensibility and specificity in ON/OFF period. In a practical system, it can be optimized by minimizing error rates with a receiver operating characteristic curve.

In this study, only one EEG and one NIRS channels were selected individually for each subject, because BCI system with small number of channels has advantages in terms of computational cost and practical use. The EEG channel, with which the best BCI command detection was achieved, was selected. Similarly, the NIRS channel was selected based on the best active/idle mode detection. Spatial SSVEP patterns which are widely distributed over the occipital were not used, although it is helpful to reduce classification errors. Analysis techniques considering multiple signals of EEG and NIRS will be discussed later.

IV. RESULTS

To validate this approach, we used the EEG and NIRS recordings to estimate the BCI commands offline. First, we will demonstrate the effect of epoch length on the performances of ON- and OFF-modes estimation using NIRS signals. Then, we will present the results obtained using the joint classification approach described previously (see Section III-C).

A. NIRS Feature Extraction

As described in Section III, NIRS signal was used to detect three possible states: "ON", "OFF", and "Unknown". Detection performance was evaluated using different epoch lengths. Epochs were extracted from all trials in ON- and OFF-periods using different time durations starting from the beginning of each period. A single epoch is extracted from each trial. Fig. 7 shows results obtained on 296 trials of ON- and OFF-periods, investigated separately. The result using only trials of ON-period is shown in Fig. 7(a), and Fig. 7(b) is for OFF-period. We define the ratio of detected trials using the three detection states as follows:

$$\text{(Ratio of detected trials)} = \frac{N_{\text{ON}} + N_{\text{OFF}}}{N_{\text{ON}} + N_{\text{OFF}} + N_{\text{Unknown}}}. \tag{12}$$

where N_{ON}, N_{OFF}, and N_{Unknown} represent number of "ON", "OFF", and "Unknown" estimation results, respectively.
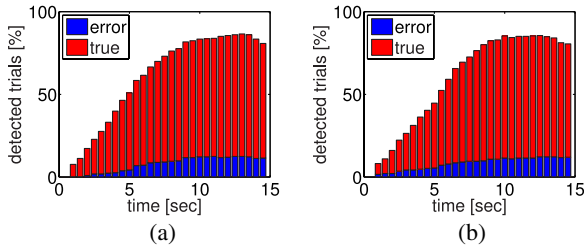
Fig. 7.   Active and idle modes detection using condition flags. The number of active and idle trials detected using NIRS increased for longer epoch lengths. It decreased slightly for epoch lengths larger than about 13 s, which may be due to attentional drops over long periods of stimulation (it is difficult for a subject to focus for long periods of time). (a) ON-period. (b) OFF-period.

These detected trials can be further subdivided into true-positives ("True" in Fig. 7) and false positives ("Error" in Fig. 7). False positives are defined as:

$$(\text{Error}) = \frac{(\text{Total of wrong estimation})}{(\text{Total of detected trials})}. \quad (13)$$

From Fig. 7, it can be observed that the number of detected trials increased with epoch time length. In both conditions, the maximum of detected trials was about 80%, most of them being correctly detected (true-positives).

B. Evaluation of Joint EEG–NIRS–BCI

This subsection presents results obtained with the joint EEG–NIRS classifier (defined in Section III-C). Before discussing the overall results, we will first of all present results pertaining to data gathered in a single block (eight ON-periods and eight OFF-periods). As was done for the study presented previously in Section IV-A, ON- and OFF-periods trials were investigated separately.

We compared the results obtained using only EEG-based detection against the results obtained using a joint EEG–NIRS classifier. Eight commands and the idle mode (total of nine classes) were estimated. Detection results are shown in Fig. 8. In this investigation, NIRS-10 and EEG-3 were selected as the most relevant channels and only these channels were used. Selected channels with the best classification performance for each subject were summarized in Table II. As expected, the error using the EEG-based classifier was higher for offset events using TH1 compared to TH2, and conversely the error was higher for onset events using TH2 compared to TH1. When using the joint EEG–NIRS classifier, the error decreased for OFF-period when using TH1, and for ON-period when using TH2. These results are summarized in Tables III and IV. For both TH1 and TH2, error decreased with longer time epochs. Moreover, performance is improved for longer time epochs. Using NIRS features, the lowest error from Table III was 6% for a 9 s time epoch and TH1. In this case, comparing an EEG-based classification against a joint EEG–NIRS classification, the error decreased by 11%.

The same investigation was performed on the whole database. Results are summarized in Fig. 9 and Tables V and VI. In Fig. 9, similar characteristics were observed as the results obtained using the single block data. As shown in Fig. 9(a2) and (b1),

errors were improved when using the joint EEG–NIRS classifier. It can be observed that events were estimated correctly by NIRS and the incidence of false positive onset or offset events was decreased. According to the averaged performances for each threshold, TH2 induced better classification results than TH1 (see Table V). Indeed, using TH2 percentages of errors were decreased of 96%, 85%, 76%, 58%, and 53% for epoch lengths of 1, 3, 5, 9, and 12 s, respectively.

Furthermore, the performance of our BCI system was assessed on the basis of the Shannon's information transfer rate (ITR). For equiprobable user commands C and s commands performed per minute, where each command was correctly decoded with equal probability p, ITR is given by the following equation:

$$\text{ITR} = s[\log_2(C) + p\log_2(p) + (1-p)\log_2(\frac{1-p}{C-1})]. \quad (14)$$

ITRs were evaluated offline as shown in Tables VII and VIII. We considered the epoch duration as an estimate of the "activation delay". With eight commands and an idle mode ($C = 9$), p varies depending on the classification errors from Table V. Because the inclusion of the idle mode slows down our BCI system, we obtained a rather slow ITR. Nevertheless, our approach of joint EEG–NIRS classification clearly improves ITRs, notably, for epoch durations of 1 and 3 s.

V. DISCUSSIONS

Current progress shows that NIRS features effectively improve BCI performance not only for motor imagery but also for SSVEP. Previous studies shown in Table I revealed that blood oxygenation responses are useful especially for a sensory motor rhythm based BCI. Such hemodynamic responses to visual stimulation were investigated mostly in fMRI studies. It was seldom investigated with NIRS. From our experimental results, hemodynamic responses recorded with NIRS can improve SSVEP-based BCI. Our hypothesis was that hemodynamic changes may be a promising indicator to overcome the limitations of the command detection based on short time epochs, and of false positives during the OFF-period. In these two aspects, EEG–BCI was actually improved with inclusion of NIRS features. Bimodal recording using EEG and NIRS can improve existing EEG–BCI performances. Furthermore, reaching beyond the specific goals of this study, we point out several approaches for further improvement of NIRS analysis, especially regarding online NIRS based BCI.

First, noise reduction may be the most important preprocessing step in the extraction of NIRS features. We applied a simple low-pass filter, which could be improved using more advanced processing techniques (such as adaptive filtering and wavelet filtering as discussed in Section II). Indeed, noise patterns varied between subjects, and nonlinear components were present such as body movement, heart rate, and respiration effects. Moreover, spatial distribution considering multiple signals will be useful to reduce classification errors in both aspects of EEG-based command estimation and of NIRS-based active/idle mode detection. Spatial SSVEP patterns in EEG have been investigated
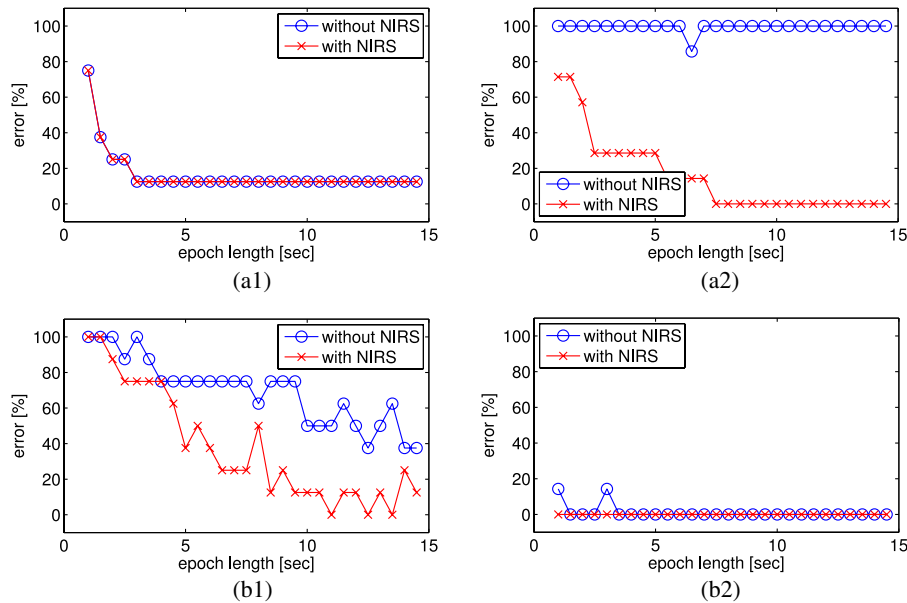
Fig. 8.   BCI command detection errors [%] were calculated using one single block. Errors obtained with (red) or without (blue) taking into account the information provided by NIRS are shown, depending on the epoch length. In (a1) and (a2), TH1 was applied for SSVEP estimation. Errors decreased when the joint EEG–NIRS classifier was used during the OFF-period. In (b1) and (b2), TH2 was applied for SSVEP estimation. Errors decreased when the joint EEG–NIRS classifier was used especially during the ON-period. In all cases, the active and the idle modes estimation was useful to decrease false positives during both ON- and OFF-periods. (a1) TH1, ON-period. (a2) TH1, OFF-period. (b1) TH2, ON-period. (b2) TH2, OFF-period.
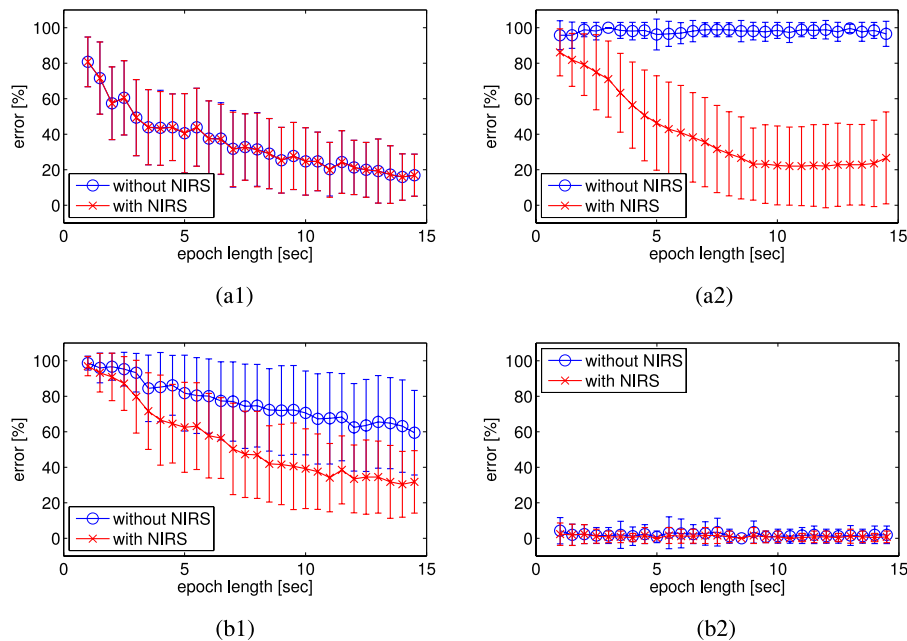
Fig. 9.   BCI command detection errors [%] were calculated using the whole database. The average errors obtained with (red) or without (blue) taking into account the information provided by NIRS are shown, depending on the epoch length. Vertical lines represent the standard deviation. In (a1) and (a2), TH1 was applied for command estimation. Errors decreased when the joint EEG–NIRS classifier was used during the OFF-period. In (b1) and (b2), TH2 was applied for SSVEP estimation. Errors decreased when the joint EEG–NIRS classifier was used during the ON-period. In all cases, the active and the idle modes estimation was useful to decrease false positives during both ON- and OFF-periods. (a1) TH1, ON-period. (a2) TH1, OFF-period. (b1) TH2, ON-period. (b2) TH2, OFF-period.

in many studies. Friman *et al.* investigated six different spatial signal processing techniques, and concluded that the minimum energy combination was the most useful method [36]. In more recent years, some advanced techniques, such as a regularized common spatial patterns (CSP) [37] and the analytic CSP [38], have been proposed. Compared to EEG analysis, there are fewer studies in NIRS analysis. Most of them selected only a region of interest (ROI) in which task related patterns are appeared. For further improvement, signal processing using ROI and nonROI simultaneously should be developed.

Detection time is the main bottleneck for BCI systems. ITRs are being severely constrained by the command detection rate; in

TABLE II
SELECTED EEG AND NIRS CHANNELS WITH THE BEST CLASSIFICATION
PERFORMANCE FOR EACH SUBJECT

Subject	EEG channel	NIRS channel
1	4	13
2	3	8
3	2	8
4	4	10
5	3	12
6	1	8
7	3	14
8	2	15
9	2	8
10	1	7
11	4	9
12	4	12
13	2	6

TABLE III
SUMMARY OF JOINT BCI COMMAND ESTIMATION RESULTS [%], AS SHOWN
IN FIG. 8

Time epoch [sec]	TH1 (lower threshold)			TH2 (higer threshold)		
	ON	OFF	All	ON	OFF	All
1	75	71	74	100	0	50
3	13	29	20	75	0	30
5	13	29	20	39	0	19
9	13	0	6	25	0	13
12	13	0	6	12	0	6

The average of the errors [%] is shown in the "All" column.

TABLE IV
SUMMARY OF COMMAND ESTIMATION IMPROVEMENT [%] BY NIRS,
AS SHOWN IN FIG. 8

Time epoch [sec]	TH1 (lower threshold)			TH2 (higer threshold)		
	ON	OFF	All	ON	OFF	All
1	100	71	84	100	0	88
3	100	29	36	75	0	60
5	100	29	36	52	0	50
9	100	0	11	33	0	34
12	100	0	11	24	0	24

Improvement is expressed as ratio of the error calculated with the joint EEG–NIRS
classifier to the error with the EEG analysis only.

TABLE V
SUMMARY OF JOINT BCI COMMAND ESTIMATION RESULTS [%], AS SHOWN IN
FIG. 9

Time epoch [sec]	TH1 (lower threshold)			TH2 (higer threshold)		
	ON	OFF	All	ON	OFF	All
1	81	86	83	97	2	49
3	49	71	61	79	1	40
5	41	46	43	63	0	31
9	25	23	25	42	1	22
12	21	22	22	33	1	17

TABLE VI
SUMMARY OF COMMAND ESTIMATION IMPROVEMENT [%], AS SHOWN IN FIG. 9

Time epoch [sec]	TH1 (lower threshold)			TH2 (higer threshold)		
	ON	OFF	All	ON	OFF	All
1	100	90	94	98	50	96
3	100	71	81	85	50	85
5	100	48	63	77	0	76
9	100	23	40	58	33	58
12	100	22	37	52	100	53

Improvement is expressed as ratio of the error calculated with the joint EEG–NIRS
classifier to the error with the EEG analysis only.

TABLE VII
INFORMATION TRANSFER RATES (ITR) FOR NINE COMMANDS INCLUDING THE
IDLE MODE, CORRESPONDING TO ALL SETS IN TABLE V

Time epoch [sec]	TH1	TH2
1	1.33	42.01
3	7.50	19.98
5	10.73	16.16
9	10.78	11.67
12	8.75	10.01

The values in each cell represent the ITR when
using EEG and NIRS features.

TABLE VIII
IMPROVEMENT OF INFORMATION TRANSFER RATES (ITR) WITH INCLUSION
OF NIRS FEATURES [%]

Time epoch [sec]	TH1	TH2
1	43.3	1.1
3	21.4	1.3
5	4.0	1.4
9	4.4	1.6
12	4.4	1.5

Improvement is expressed as ratio of the
ITR with the joint EEG–NIRS classifier
to the ITR with the EEG analysis only.
The ITR wasimproved successfully even
though only one NIRS channel was used.

order to develop an efficient BCI system, NIRS features should be correctly detected within a time interval as short as 2–3 s. In this and previous studies, slow NIRS oscillations at the beginning and at the end of stimulation are observed. However, these responses were delayed by 2–3 s after the neural activity—therefore, a simple measurement of the NIRS signal amplitude is of limited interest (too slow) for BCI systems. We presented here an approach based on signal derivatives, and demonstrated its usefulness for the fast detection of NIRS responses. However, caution is necessary since this measure is sensitive to high frequency noise components. Preprocessing of artifacts is necessary to ensure the detection quality, which is why we removed higher frequency components with a low-pass filter. However, these frequency components, as well as the information from the rejected channels—which we did not use in this analysis—may also contain valuable information. Therefore, there is still room for improvements.

One limit of our study is the stimulation protocol used. NIRS feature extraction could be tested using different time ranges of stimulation, but for practical reasons, we could only record fixed epochs of 15 s in our study. Despite this approach allowed us to collect interesting data, in practical applications for an online BCI system, the NIRS response may change depending on the stimulation time. In addition, the use of NIRS features to detect idle modes on short intervals should only be done with proper care. Indeed, the estimated flags may cause false positives when a subject focuses on the SSVEP stimulation for too short a time (< 2–3 s). To circumvent that risk, we suggestthat a threshold could be adapted to the second derivative depending on the epoch length, in that case, oscillations with too low amplitudes could be ignored.

Finally, our proposed methodology can be applied to other modalities such as a motor imagery task. Although NIRS signals have lower time resolution than EEG signals, it can be used to reduce false positives.

VI. CONCLUSION

In this study, we propose an integrated signal processing approach for a new dual-modality or joint EEG–NIRS–BCI based on the SSVEP paradigm which improved the performances as compared to an EEG-only BCI. Our method addressed some important drawbacks of EEG-based BCI designs by reducing the required epoch lengths and the false positive commands during periods when the subject is not executing any command (OFF-period). The classification error for nine classes, including eight commands and an idle state output, were decreased with the inclusion of NIRS features. For 13 subjects, nine class estimation errors for 3, 5, 9, 12-s epochs were 40%, 31%, 22%, and 17%, respectively. In each time epoch, improved error ratios by NIRS (error with NIRS to error without NIRS) were 85%, 76%, 58%, and 53%, respectively. These results were obtained from only one EEG and one NIRS channel. It is possible for future studies to improve further the proposed NIRS feature extraction especially by optimizing artifact removal techniques.

REFERENCES

[1] E. Fetz, "Operant conditioning of cortical unit activity," *Science*, vol. 163, no. 3870, pp. 955–958, 1969.

[2] N. Birbaumer, "Breaking the silence: Brain–computer interfaces (BCI) for communication and motor control," *Psychophysiology*, vol. 43, no. 6, pp. 517–532, Nov. 2006.

[3] N. Birbaumer and L. G. Cohen, "Brain–computer interfaces: Communication and restoration of movement in paralysis," *J. Physiol.*, vol. 579, no. 3, pp. 621–636, Mar. 2007.

[4] J. R. Wolpaw, N. Birbaumer, D. J. McFarland, G. Pfurtscheller, and T. M. Vaughan, "Brain–computer interfaces for communication and control," *Clin. Neurophysiol.: Offic. J. Int. Federat. Clin. Neurophysiol.*, vol. 113, no. 6, pp. 767–791, Jun. 2002.

[5] B.-K. Min, M. J. Marzelli, and S.-S. Yoo, "Neuroimaging-based approaches in the brain-computer interface," *Trends Biotechnol.*, vol. 28, no. 11, pp. 552–560, Nov. 2010.

[6] C. Brunner and R. Leeb, (2014, Jan. 26). BCI Competition 2008—Graz data set A. [Online]. Available: http://www.bbci.de/competition/iv/desc_2a.pdf

[7] H. Bakardjian. (2014, Jan. 26). SSVEP database (EEG) [Online]. Available: http://www.bsp.brain.riken.jp/~hova/ssvep_data_Bakardjian_LABSP.html

[8] S. Sanei and J. A. Chambers, *EEG Signal Processing.* London, U.K.: Wiley, 2007.

[9] A. Bashashati, M. Fatourechi, R. K. Ward, and G. E. Birch, "A survey of signal processing algorithms in brain-computer interfaces based on electrical brain signals," *J. Neural Eng.*, vol. 4, no. 2, pp. R32–57, Jun. 2007.

[10] F. Lotte, M. Congedo, A. Lécuyer, F. Lamarche, and B. Arnaldi, "A review of classification algorithms for EEG-based brain–computer interfaces," *J. Neural Eng.*, vol. 4, no. 2, pp. R1–R13, Jun. 2007.

[11] N. J. Hill, T. N. Lal, M. Schr, T. Hinterberger, G. Widman, C. E. Elger, B. Sch, and N. Birbaumer, "Classifying event-related desynchronization in EEG, ECoG and MEG signals," *Lecture Notes Comput. Sci.*, vol. 4174, pp. 404–413, 2006.

[12] J. D. R. Millan, J. Mourino, M. Franze, F. Cincotti, M. Varsta, J. Heikkonen, and F. Babiloni, "A local neural classifier for the recognition of EEG patterns associated with mental tasks," *IEEE Trans. Neural Netw./Publicat. IEEE Neural Netw. Council*, vol. 13, no. 3, pp. 678–86, Jan. 2002.

[13] M. Thulasidas, C. Guan, and J. Wu, "Robust Classification of EEG Signal for Brain-Computer Interface," *IEEE Trans. Neural Syst. Rehabil. Eng.: Publicat. IEEE Eng. Med. Biol. Soc.*, vol. 14, no. 1, pp. 24–29, Mar. 2006.

[14] Z. Lin, C. Zhang, W. Wu, and X. Gao, "Frequency recognition based on canonical correlation analysis for SSVEP-based BCIs," *IEEE Trans. Biomed. Eng.*, vol. 54, no. 6, pp. 1172–1176, Jun. 2007.

[15] Y. Wang, X. Gao, B. Hong, C. Jia, and S. Gao, "Brain–computer interfaces based on visual evoked potentials," *IEEE Eng. Med. Biol. Mag.: Quart. Mag. Eng. Med. Biol. Soc.*, vol. 27, no. 5, pp. 64–71, Sep./Oct. 2008.

[16] F.-B. Vialatte, M. Maurice, J. Dauwels, and A. Cichocki, "Steady-state visually evoked potentials: Focus on essential paradigms and future perspectives," *Prog. Neurobiol.*, vol. 90, no. 4, pp. 418–438, Apr. 2010.

[17] H. Bakardjian, T. Tanaka, and A. Cichocki, "Optimization of SSVEP brain responses with application to eight-command brain–computer interface," *Neurosci. Lett.*, vol. 469, no. 1, pp. 34–38, Jan. 2010.

[18] G. Pfurtscheller, B. Z. Allison, C. Brunner, G. Bauernfeind, T. Solis-Escalante, R. Scherer, T. O. Zander, G. Mueller-Putz, C. Neuper, and N. Birbaumer, "The hybrid BCI," *Front. Neurosci.*, vol. 4, no. April, Jan. 2010.

[19] S. Coyle, T. Ward, C. Markham, and G. McDarby, "On the suitability of near-infrared (NIR) systems for next-generation brain-computer interfaces," *Physiol. Meas.*, vol. 25, no. 4, pp. 815–822, Aug. 2004.

[20] R. Sitaram, H. Zhang, C. Guan, M. Thulasidas, Y. Hoshi, A. Ishikawa, K. Shimizu, and N. Birbaumer, "Temporal classification of multichannel near-infrared spectroscopy signals of motor imagery for developing a brain-computer interface," *NeuroImage*, vol. 34, no. 4, pp. 1416–1427, Feb. 2007.

[21] K. Tai and T. Chau, "Single-trial classification of NIRS signals during emotional induction tasks: Towards a corporeal machine interface," *J. Neuroeng. Rehabil.*, vol. 6, p. 39, Jan. 2009.

[22] M. Takeuchi, E. Hori, K. Takamoto, A. H. Tran, K. Satoru, A. Ishikawa, T. Ono, S. Endo, and H. Nishijo, "Brain cortical mapping by simultaneous recording of functional near infrared spectroscopy and electroencephalograms from the whole brain during right median nerve stimulation," *Brain Topogr.*, vol. 22, no. 3, pp. 197–214, Nov. 2009.

[23] S. Fazli, J. Mehnert, J. Steinbrink, G. Curio, A. Villringer, K.-R. Müller, and B. Blankertz, "Enhanced performance by a hybrid NIRS–EEG brain computer interface," *NeuroImage*, vol. 59, pp. 519–529, Aug. 2011.

[24] A. M. Dale and R. L. Buckner, "Selective averaging of rapidly presented individual trials using fMRI," *Human Brain Mapp.*, vol. 5, no. 5, pp. 329–340, Jan. 1997.

[25] M. Bianciardi, L. Bianchi, G. Garreffa, M. Abbafati, M. Di Russo, M. G. Marciani, and E. Macaluso, "Single-epoch analysis of interleaved evoked potentials and fMRI responses during steady-state visual stimulation," *Clin. Neurophysiol.: Offic. J. Int. Federat. Clin. Neurophysiol.*, vol. 120, no. 4, pp. 738–747, Apr. 2009.

[26] N. K. Logothetis, J. Pauls, M. Augath, T. Trinath, and A. Oeltermann, "Neurophysiological investigation of the basis of the fMRI signal," *Nature*, vol. 412, no. 6843, pp. 150–157, Jul. 2001.

[27] Z. Liu, C. Rios, N. Zhang, L. Yang, W. Chen, and B. He, "Linear and nonlinear relationships between visual stimuli, EEG, and BOLD fMRI signals," *NeuroImage*, vol. 50, no. 3, pp. 1054–1066, Apr. 2010.

[28] T. J. Huppert, R. D. Hoge, S. G. Diamond, M. A. Franceschini, and D. A. Boas, "A temporal comparison of BOLD, ASL, and NIRS hemodynamic responses to motor stimuli in adult humans," *NeuroImage*, vol. 29, no. 2, pp. 368–382, Jan. 2006.

[29] S. P. Koch, J. Steinbrink, A. Villringer, and H. Obrig, "Synchronization between background activity and visually evoked potential is not mirrored by focal hyperoxygenation: implications for the interpretation of vascular brain imaging," *J. Neurosci.: Offic. J. Soc. Neurosci.*, vol. 26, no. 18, pp. 4940–4948, May 2006.

[30] F. Matthews, B. Pearlmutter, T. Ward, C. Soraghan, and C. Markham, "Hemodynamics for brain–computer interfaces," *IEEE Signal Process. Mag.*, vol. 25, no. 1, pp. 87–94, Jan. 2008.

[31] X.-S. Hu, K.-S. Hong, S. S. Ge, and M.-Y. Jeong, "Kalman estimator- and general linear model-based on-line brain activation mapping by near-infrared spectroscopy," *Biomed. Eng. Online*, vol. 9, no. 1, p. 82, Jan. 2010.

[32] G. Gratton and P. M. Corballis, "Removing the heart from the brain: compensation for the pulse artifact in the photon migration signal," pp. 292–299, May 1995

[33] F. C. Robertson, T. S. Douglas, and E. M. Meintjes, "Motion artifact removal for functional near infrared spectroscopy: A comparison of methods," *IEEE Trans. Biomed. Eng.*, vol. 57, no. 6, pp. 1377–1387, Jun. 2010.

[34] Q. Zhang, G. E. Strangman, and G. Ganis, "Adaptive filtering to reduce global interference in noninvasive NIRS measures of brain activation: How well and when does it work?" *NeuroImage*, vol. 45, no. 3, pp. 788–794, 2010.

[35] Q. Zhang, E. N. Brown, and G. E. Strangman, "Adaptive filtering for global interference cancellation and real-time recovery of evoked brain activity: A Monte Carlo simulation study," *J. Biomed. Opt.*, vol. 12, no. 4, pp. 044 014-1–044 014-12, 2012.

[36] O. Friman, I. Volosyak, and A. Gräser, "Multiple channel detection of steady-state visual evoked potentials for brain–computer interfaces," *IEEE Trans. Biomed. Eng.*, vol. 54, no. 4, pp. 742–750, Apr. 2007.

[37] F. Lotte and C. Guan, "Regularizing common spatial patterns to improve BCI designs: Unified theory and new algorithms," *IEEE Trans. Biomed. Eng.*, vol. 58, no. 2, pp. 355–362, Feb. 2011.

[38] O. Falzon, K. P. Camilleri, and J. Muscat, "The analytic common spatial patterns method for EEG-based BCI data," *J. Neural Eng.*, vol. 9, no. 4, p. 045009, Aug. 2012.

Authors' photographs and biographies not available at the time of publication.